Frequency-Diverse Computational Microwave Phaseless Imaging

Yurduseven, O., Fromenteze, T., Marks, D., Gollub, J., & Smith, D. (2017). Frequency-Diverse Computational Microwave Phaseless Imaging. *IEEE Antennas and Wireless Propagation Letters*, *16*, 1-4. https://doi.org/10.1109/LAWP.2017.2748139

Published in:
IEEE Antennas and Wireless Propagation Letters

Document Version:
Peer reviewed version

Queen's University Belfast - Research Portal:
Link to publication record in Queen's University Belfast Research Portal

This article has been accepted for publication in a future issue of this journal, but has not been fully edited. Content may change prior to final publication. Citation information: DOI 10.1109/LAWP.2017.2748139, IEEE Antennas and Wireless Propagation Letters

Frequency-Diverse Computational Microwave Phaseless Imaging

Okan Yurduseven, *Senior Member, IEEE*, Thomas Fromenteze, Daniel L. Marks, Jonah N. Gollub, *Member, IEEE*, and David. R. Smith, *Member, IEEE*

***Abstract*— Phaseless imaging approaches provide a significant advantage for systems where maintaining coherency during the acquisition time is difficult. Here we demonstrate a phaseless, frequency-diverse, computational imaging system that operates at K-band frequencies (17.5 – 26.5 GHz). The system consists of a cavity-backed metasurface antenna producing spatially diverse radiation patterns that vary as a function of the driving frequency. The frequency-diverse metasurface antenna can be used to form images at microwave frequencies by collecting measurements at frequencies sampled over the operational bandwidth, obviating the need for either mechanically moving parts or phase shifting circuits. We show that high-fidelity images can be obtained with the metasurface antenna using only the intensity of the measurements by leveraging a sparse variant of the Wirtinger Flow algorithm. In addition to the hardware simplification achieved by using a frequency-diverse approach, we demonstrate a significant reduction in the number of measurements required to reconstruct a given number of voxels for the phaseless imaging problem. This difference from conventional phase retrieval techniques is achieved by leveraging the sparsity concept, simplifying the complexity of the imaging problem.**

***Index Terms*—imaging, microwaves, phase retrieval, computational, metasurface.**

I. Introduction

A significant advantage of radio frequency (RF) imaging, including microwave and millimeter wave, is that electromagnetic waves in these frequency bands can penetrate through many materials that are opaque at visible wavelengths, making them suitable for applications such as security-screening [1], through-wall imaging [2], non-destructive testing [3] and biomedical imaging [4].

At RF, the control and detection of the phase of a wave is easily achieved, enabling many coherent imaging approaches that are commonly used in RF imaging. In imaging modalities such as synthetic aperture radar (SAR) and holography, phase measurement of the received wave is essential to enable image reconstruction. In the complementary approach, in which a diffraction limited beam is created that can be used to scan a target, a large and coherent aperture is needed to dynamically form and steer the beam, again requiring phase control, introducing significant complication to the system. A coherent imaging system must both detect phase and maintain phase coherency across a large aperture, requiring coherent combination of the measured data across the synthesized aperture for SAR imaging and a phase-shifting circuit to be introduced at each location where the field is sampled for phased arrays. The large number of phase shifters leads to complex and often expensive system architectures [5].

The need for coherent phase detection can be avoided using interferometric approaches. In holographic approaches, for example, phase information can be recovered from intensity-only measurements by mixing the object scattered field with a coherent reference signal. Using holographic techniques, high-fidelity phaseless imaging has been successfully demonstrated [6]. Although promising results were achieved, a major drawback with these techniques is that the measurements are done by means of a mechanical scanning process, limiting the data acquisition speed. Alternatively, a panel of transmit and receive antennas could also be adopted [7]. For large apertures, or for apertures comprising many sub-apertures, establishing phase coherency can be a challenge, introducing a need for dynamically applied phase calibration and adding another layer of complexity to the imaging process.

With the advent of computational imaging, many more coherent and incoherent imaging scenarios become feasible; hardware constraints on the aperture and RF backend can be relaxed, with processing time and availability of stable reconstruction algorithms becoming the major limitations. In a computational imaging system, the role of the aperture is to acquire a set of measurements of a scene that contain sufficient information to reconstruct images at the desired fidelity. The computational imaging approach we consider here is based on a frequency-diverse, metasurface aperture [8]-[12]. The frequency-diverse aperture consists of a cavity-backed array of radiating metamaterial elements—often simple irises—which produce unique and complex spatial field patterns that vary as a function of the driving frequency. From a set of complex (phase and amplitude) measurements taken at many different frequencies, an image can be reconstructed using computational imaging algorithms. The frequency-diverse imager is advantageous in that it requires no moving parts, and only a single source and detector pair.

Manuscript received August 07, 2017; accepted August 29, 2017.

O. Yurduseven, D. L. Marks, J. N. Gollub, and D. R. Smith are with the Center for Metamaterials and Integrated Plasmonics, Department of Electrical and Computer Engineering, Duke University, Durham, North Carolina, 27708, USA (email: okanyurduseven@ieee.org).

T. Fromenteze is with the Xlim Research Institute, University of Limoges, 87060 Limoges, France.

This article has been accepted for publication in a future issue of this journal, but has not been fully edited. Content may change prior to final publication. Citation information: DOI 10.1109/LAWP.2017.2748139, IEEE Antennas and Wireless Propagation Letters

While many examples of frequency-diverse imaging have been presented previously [8]-[12], the systems demonstrated have made use of coherent (phase-sensitive) detection schemes. In principle, however, acquisition of the phase is not necessary and can be avoided. A proof-of-concept experiment showing the phaseless localization of a point source was achieved recently using a frequency-diverse antenna [13] in conjunction with the Truncated Wirtinger Flow (WF) reconstruction algorithm [14]. The implementation of the WF technique in [13]—which provides a means of solving the quadratic problem arising in a one-way localization scenario—was mainly limited by the ratio between the number of measurements (M) and the number of voxels (N) forming the scene to be reconstructed; for stable reconstruction that ratio is typically on the order of or greater than M/N=5. The significant oversampling leads to long reconstruction times and cumbersome implementations.

In the present work, we demonstrate that more recent Sparse WF algorithm [15] significantly relaxes the constraint on the M/N ratio. Using the sparsity property of the reconstructed scenes, we demonstrate high-fidelity phaseless imaging with an M/N ratio of as small as M/N=0.8. The presented system exhibits the first implementation of a phaseless imaging problem from intensity-only measurements taken using a frequency-diverse computational imaging system operating at microwave frequencies.

II. Phaseless Frequency-Diverse Computational Imaging and Phase Retrieval

The concept of frequency-diverse imaging relies on the use of frequency-dependent radiation patterns to encode the scene information onto a set of measurement modes from which the scene is reconstructed using computational imaging algorithms [8]-[12]. The scene is correlated to the measurements through a forward model expressed as

$$\mathbf{g} = \mathbf{H}\mathbf{f} + \mathbf{n} \tag{1}$$

where $\mathbf{g}$ denotes the measurement vector; $\mathbf{H}$ is the measurement (or sensing) matrix; $\mathbf{f}$ is the scene vector to be reconstructed; and, $\mathbf{n}$ is the measurement noise. In (1) bold font is adopted for vector-matrix notation. For a frequency-diverse imaging system supporting M measurement modes and a scene discretized into N voxels, $\mathbf{g}$ has dimension Mx1 while $\mathbf{H}$ and $\mathbf{f}$ have dimensions MxN and Nx1, respectively. Within the first Born approximation, the elements of the measurement matrix $\mathbf{H}$ consist of the product of the fields radiated by the transmit (E_{Tx}) and receive (E_{Rx}) antennas at a given point in the scene, or $\mathbf{H}(\omega)=E_{\mathrm{Tx}}(\omega, \mathbf{r})E_{\mathrm{Rx}}(\omega, \mathbf{r})$ [11].

To demonstrate the imaging technique, we use the frequency-diverse imaging system shown in Fig. 1, which consists of a single metasurface cavity-backed antenna connected to two measurement ports using ultrawide bandwidth probes. The aperture thus functions as a transceiver (monostatic imaging), with both the transmit and receive fields taken at the location of the antenna aperture. The cavity is fed at one port of the antenna and the signal received at the second port of the antenna. The source and detector for the experiments is a vector network analyzer (VNA, Agilent N5245A). The VNA provides both the phase and amplitude for the measured fields, allowing the comparison of phaseless retrieval with those using phase.

The surface of the cavity antenna is patterned using an array of subwavelength irises. These irises couple to the frequency-dependent cavity modes within the cavity, resulting in frequency-dependent radiation patterns. If the K-band (17.5 – 26.5 GHz) is sampled at M frequency points, the number of measurement modes is no greater than M. However, if the radiation patterns contain significant spatial correlation, the effective number of measurement modes may be considerably fewer than M. From a rigorous analysis of the cavity-backed metasurface antenna, it can be determined that the maximum number of supported measurement modes is directly proportional to the quality (Q) factor of the antenna [8]. A frequency-diverse antenna with a large Q-factor can produce highly orthogonal radiation patterns (with minimum spatial overlap) even when the frequency sampling interval, Δf is selected to be extremely small. The Q-factor of the metasurface cavity antenna in this work is Q=12000, supporting an upper-bound of M=4900 measurement modes [8]. In this work, we choose M to be M=4001, slightly under the upper-bound limit.

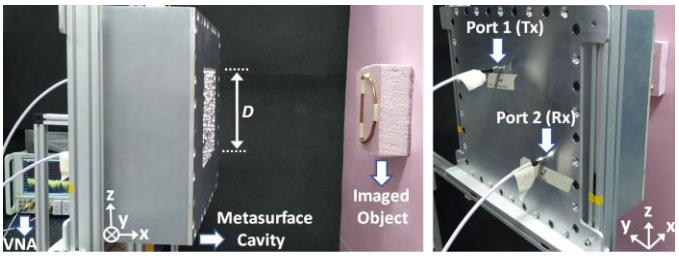

(a) (b)

Fig. 1. Frequency-diverse imaging system (a) side-view (b) back-view. The target is at a distance of x=25 cm. D=16 cm.

In the formulation of Eq. (1), the $\mathbf{g}$ is a measurement vector consisting of complex components. If both the phase and amplitude are accessible, $\mathbf{g}$ can be obtained directly and the reflectivity distribution, $\mathbf{f}$, can be estimated using straightforward methods such as matched filter or least squares [12]. Because the measurement modes are typically neither complete nor orthogonal, only an estimate of $\mathbf{f}$ can be found, $\mathbf{f}_{est}$, which can be obtained from $\mathbf{f}_{est} = \arg\min_{f} \left(\|\mathbf{g} - \mathbf{H}\mathbf{f}\|_2 \right)$; (1) thus leads to a convex problem that converges well using iterative solvers. For phaseless reconstruction, our goal is to estimate $\mathbf{f}$ from a set of intensity measurements of the form

$$\mathbf{g}_{\mathrm{int}} = \left| \mathbf{H}\mathbf{f} + \mathbf{n} \right|^2 \tag{2}$$

It is evident that (2) is quadratic, constitutes a non-convex minimization problem and exhibits ambiguous solutions [16]. Reconstruction methods available for phase-resolved measurements—such as pseudo-inverse, matched filter and least-squares—therefore cannot be leveraged to solve (2).

A number of techniques have been suggested to solve the problem posed by (2) [14], [16]. The Truncated WF algorithm, for example, is one approach that has been shown to be efficient, though implementations have typically required an

This article has been accepted for publication in a future issue of this journal, but has not been fully edited. Content may change prior to final publication. Citation information: DOI 10.1109/LAWP.2017.2748139, IEEE Antennas and Wireless Propagation Letters

excess of measurements as compared with the number of voxels required for reconstruction [13]. To minimize the number of measurements taken for a given image, additional constraints can be imposed that restrict the number of possible solutions of **f** that minimize the phaseless objective function.

In typical imaging scenarios, the imaged objects do not occupy the entire scene but rather a sub-section of it, enabling (2) to be considered a sparse phase retrieval problem, that is $||\mathbf{f}_{est}||_0=k$, where k denotes the number of non-zero elements in $\mathbf{f}_{est}$. The Sparse WF algorithm can be considered a two-step phase retrieval technique [15]. The first step involves estimating the signal support using the power spectrum of the scene which is proportional to the product of the intensity of the measured signal and the squared measurement matrix. The support is determined by taking the k largest portion of this spectrum. This is followed by an initialization process where a truncated spectral method is applied to calculate an estimation of the scene (over the restricted support) for the phaseless imaging problem. In the second step, the initial estimate of the scene (over the restricted support) is constantly iterated using a hard thresholding gradient-descent method, calculating

$$\mathbf{f}_{est}^{(t+1)} = \mathbf{f}_{est}^{(t)} - \frac{\mu}{\phi^2}\nabla\mathbf{f}_{est}^{(t)} \tag{3}$$

where μ is the step size, $\phi = 1/M \sum_{i=1}^{M} \mathbf{g}_{\text{int}}^{i}$ and $\nabla\mathbf{f}_{est}^{t}$ is calculated using the Wirtinger derivative in (4) where † operator denotes the conjugate transpose. If $\mathbf{h}_i$ represents the individual row vectors of the measurement matrix **H**, where $i = 1 \to M$, then

$$\nabla\mathbf{f}_{est} = \frac{2}{M}\sum_{i=1}^{M}((\mathbf{h}_i^{\dagger}\mathbf{f}_{est})^2 - \mathbf{g}_{\text{int}})\mathbf{h}_i\mathbf{h}_i^{\dagger}\mathbf{f}_{est} \tag{4}$$

At each iteration of the gradient-descent algorithm, a gradient of $\mathbf{f}_{est}$ from the prior iteration is calculated using (4). This step reveals the direction in which the algorithm moves to converge to the minima by an amount governed by the step size, μ. This process is repeated until the convergence is achieved. The gradient-descent algorithm is a hard thresholding based technique, keeping the k largest absolute values of the estimated solution at each iteration [15]. Once the algorithm reaches the minimum, theoretically, the gradient in (4), $\nabla\mathbf{f}_{est}^{(t)}$, equals zero, resulting in $\mathbf{f}_{est}^{(t+1)} = \mathbf{f}_{est}^{(t)}$, thus the algorithm is terminated. In practice, the termination criterion was the number of iterations, which was selected to be 100 as a result of the parametric analyses performed on the convergence of the algorithm. It should be noted that, in comparison to single-shot reconstruction algorithms available for complex amplitude measurements, such as pseudo-inverse and matched-filter [12], the reconstruction time for phaseless imaging is longer due to the iterative nature of the retrieval problem. This aspect will be quantitively discussed in the next section.

III. Imaging Results and Discussion

Using the frequency-diverse imaging system shown in Fig. 1, we first image a point-target, from which we obtain the point spread function (PSF) [12]. For this analysis, we make use of a set of MATLAB-based codes, referred to here as the Virtualizer [11], which is capable of modeling the imaging performance of arbitrary metasurface apertures. In the Virtualizer, the aperture fields are replaced by an array of magnetic dipoles, with the fields radiated by each dipole propagated to the scene using the appropriate Green's function. The scene is discretized into collections of three-dimensional (3D) voxels. The dimensions of the voxels are selected to be 1.5 cm in cross-range (*yz*-plane) and 1.5 cm in range (*x*-axis)—values in accordance with the theoretical resolution limits of the imager (1.8 cm in cross-range and 1.67 cm in rage, respectively) calculated using standard radar resolution equations [12]. Image reconstruction is done in two ways; first, complex amplitude based and second, phaseless. For complex amplitude imaging, we make use of the complex measured signal, **g** in (1), and reconstruct the scene using the matched-filter technique, $\mathbf{f}_{est}=\mathbf{H}^{\dagger}\mathbf{g}$, where $\mathbf{H}^{\dagger}$ denotes the conjugate transpose of **H**. For phaseless imaging, we make use of the intensity of the measured signal, $\mathbf{g}_{int}$ in (2), and reconstruct the scene using the Sparse WF algorithm. The reconstructed PSF patterns decomposed into cross-range and range are shown in Fig. 2 (*M*/*N* ratio is 0.8).

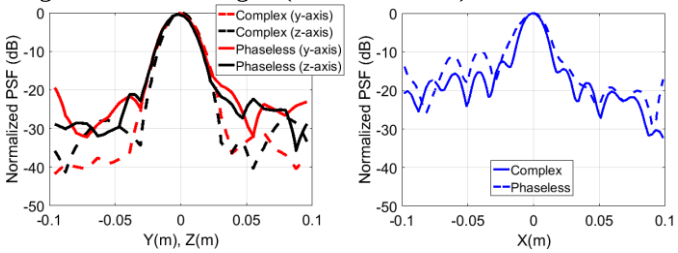

(a) (b)

Fig. 2. PSF patterns (a) cross-range (b) range.

The PSF patterns reconstructed using the phaseless algorithm exhibit good agreement with the complex reconstructed PSF patterns. The phaseless reconstructed PSF patterns in the range and cross-range planes have more prominent sidelobes. This is expected, especially in the range plane as the range information is encoded by phase, which is not measured directly but retrieved through the retrieval algorithm. The overall sidelobe levels for the phaseless reconstructed PSF patterns remain below -20 dB in cross-range and -10 dB in range. Observing the -3dB full-width-half-maximum (FWHM) values in cross-range and range, the resolution limits of the aperture are calculated to be 2 cm in cross-range and 1.7 cm in range, exhibiting good agreement with the theoretical limits noted above. To demonstrate the imaging of more complex targets, we formed the individual letter "D" of "DUKE" using copper wires. Image reconstruction was again performed using the complex measurement vector, **g** in (1), and the intensity-only measurement vector, $\mathbf{g}_{int}$ in (2). The complex measurement based reconstructed image of the letter is shown in Fig. 3(a) while the phaseless reconstruction is illustrated in Fig. 3(b). It should be noted that although the reconstructions are three-dimensional (3D), in Fig. 3, front projections are shown. Analyzing Fig. 3, it can be seen that both the complex measurement based and phaseless reconstructions reveal a clear

This article has been accepted for publication in a future issue of this journal, but has not been fully edited. Content may change prior to final publication. Citation information: DOI 10.1109/LAWP.2017.2748139, IEEE Antennas and Wireless Propagation Letters

outline of the imaged object. The normalized mean square error between the complex measurement based and phaseless reconstructed images remains below 10%. We also demonstrate the phaseless reconstruction of the letter "D" using the conventional non-Sparse WF algorithm [13], [14] in Fig. 3(c). It is evident that when M/N=0.8 the reconstruction fails. The actual imaged object is shown as an inset in Fig. 3.

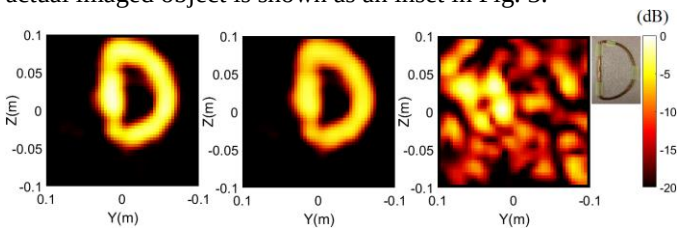

(a) (b) (c)

Fig. 3. Reconstruction of letter "D" (M/N=0.8) (a) complex-measurement; phaseless (b) Sparse WF (c) non-Sparse WF.

Another important metric for imaging is the reconstruction time, which was measured to be 0.012 s for the complex based imaging in Fig. 3(a) (matched-filter reconstruction) and 6.6 s for the phaseless imaging in Fig. 3(b). This difference is expected as the phaseless imaging is not a single-shot reconstruction technique but consists of an iterative retrieval process. However, a significant advantage of employing the sparsity relaxation for the phaseless imaging problem can be appreciated by measuring the reconstruction time using the non-Sparse WF algorithm, satisfying M/N=5 convergence criterion, which was measured to be 20 s, almost three times longer than the system presented in this work. Currently the phaseless retrieval algorithm is run on a central processing unit (CPU, Intel Xeon e5). Parallelizing the retrieval problem using graphics processing units (GPUs) can significantly reduce the reconstruction time [17]. This is an ongoing research effort.

Finally, to analyze the convergence characteristics, we study the lower bound limit of the M/N ratio for the Sparse WF algorithm. For this study, we vary the M/N ratio from 0.3 to 0.8; M_1/N_1=0.3, M_2/N_2=0.6 and M_3/N_3=0.8. The reconstructed images as a function varying M/N ratio are shown in Fig. 4.

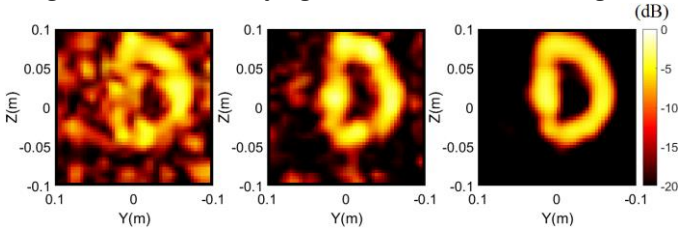

(a) (b) (c)

Fig. 4. Phaseless reconstruction of the letter "D" (a) M_1/N_1=0.3 (b) M_2/N_2=0.6 (c) M_3/N_3=0.8.

Analyzing Fig. 4, the lower-bound limit to achieve a successful convergence for the phaseless imaging is determined to be M/N>0.6, in good agreement with the analysis presented in [15]. In comparison to the complex based reconstruction of Fig. 3(a), the normalized mean square error was calculated to be 48% for M_1/N_1=0.3, 23% for M_2/N_2=0.6, and 8% for M_3/N_3=0.8, respectively. No consistent solution exists for the phaseless reconstruction problem below M/N=0.3 limit.

IV. Conclusion

We have demonstrated a phaseless imaging system consisting of a frequency-diverse metasurface cavity antenna operating at K-band frequencies. Phaseless imaging makes it possible to recover scene information from simple intensity-only measurements. Leveraging the Sparse WF algorithm, significant relaxation on the M/N constraint for successful convergence has been achieved. The phaseless images reconstructed using the Sparse WF algorithm with M/N=0.8 are on par with the complex measurement based reconstructions. The proposed phaseless frequency-diverse imaging system circumvents the requirement for phase synthetization in measurements and can readily be scaled to higher frequencies.

Acknowledgment

This work was supported by the Air Force Office of Scientific Research (AFOSR, Grant No. FA9550-12-1-0491).

References

[1] B. Gonzalez-Valdes *et al*., "Millimeter Wave Imaging Architecture for On-The-Move Whole Body Imaging," *IEEE Trans. Antennas Propag.*, vol. 64, no. 6, pp. 2328-2338, 2016.

[2] W. Yazhou, and A. E. Fathy, "Advanced system level simulation platform for three-dimensional UWB through-wall imaging SAR using time-domain approach," *IEEE Trans. Geosci. Rem. Sens.*, vol. 50, no. 5, pp. 1986-2000, 2012.

[3] S. Kharkovsky and R. Zoughi, "Microwave and millimeter wave nondestructive testing and evaluation - Overview and recent advances," *IEEE Instr. Measur. Mag.*, vol. 10, no. 2, pp. 26-38, 2007.

[4] N. K. Nikolova, "Microwave imaging for breast cancer," IEEE Microw. Mag., 2011, 12, no. 7, pp. 78-94.

[5] R. C. Hansen, *Phased array antennas*, 2nd ed., Hoboken, NJ, USA: John Wiley & Sons, 2009.

[6] D. Smith, O. Yurduseven, B. Livingstone and V. Schejbal, "Microwave imaging using indirect holographic techniques," *IEEE Antennas Propag. Mag.*, vol. 56, no. 1, pp. 104-117, 2014.

[7] J. Laviada, *et al.*, "Phaseless Synthetic Aperture Radar with Efficient Sampling for Broadband Near-Field Imaging: Theory and Validation," *IEEE Trans. Antennas Propag.*, vol. 63, no. 2, pp. 573-584, 2015.

[8] D. L. Marks, J. Gollub, and D. R. Smith, "Spatially resolving antenna arrays using frequency diversity," *J. Opt. Soc. Am. A*, vol. 33, no. 5, pp. 899-912, 2016.

[9] O. Yurduseven, V. R. Gowda, J. N. Gollub and D. R. Smith, "Printed aperiodic cavity for computational and microwave Imaging," *IEEE Microw. Compon. Lett.*, vol. 26, no. 5, pp. 367-369, 2016.

[10] T. Fromenteze, O. Yurduseven, M. F. Imani, J. Gollub, C. Decroze, D. Carsenat, and D. R. Smith, "Computational imaging using a mode-mixing cavity at microwave frequencies," *Applied Physics Letters*, vol. 106, no. 19, p. 194104, 2015.

[11] G. Lipworth, *et al.*, "Comprehensive simulation platform for a metamaterial imaging system," *Appl. Opt*., vol. 54, pp. 9343-9353, 2015.

[12] O. Yurduseven, *et al*, "Resolution of the frequency diverse metamaterial aperture imager," *Prog. Electromagnetics Res.*, vol. 150, pp. 97-107, 2015.

[13] T. Fromenteze, X. Liu, M. Boyarsky, J. Gollub, and D. R. Smith, "Phaseless computational imaging with a radiating metasurface," *Opt. Express*, vol. 24, pp. 16760-16776, 2016.

[14] Y. Chen and E. Candes, "Solving random quadratic systems of equations is nearly as easy as solving linear systems," *Advances in Neural Information Processing Systems*, pp. 739–747, 2015.

[15] Z. Yuan, Q. Wang, and H. Wang, "Phase retrieval via Sparse Wirtinger Flow," Arxiv: 1704.03286v1, 2017.

[16] I. S. Stefanescu, "On the phase retrieval problem in two dimensions," *J. Math. Phys.*, vol. 26, pp. 2141-2160, 1985.

[17] D. L. Marks, O. Yurduseven and D. R. Smith, "Fourier Accelerated Multistatic Imaging: A Fast Reconstruction Algorithm for Multiple-Input-Multiple-Output Radar Imaging," *IEEE Access*, vol. 5, pp. 1796-1809, 2017.